



Effects of Inclined Volute Tongue Structure on the Internal Complex Flow and Aerodynamic Performance of the Multi-Blade Centrifugal Fan

Y. Wei^{†1}, J. Wang¹, J. Xu², Z. Wang¹, J. Luo¹, H. Yang¹, Z. Zhu¹ and W. Zhang¹

¹National-Provincial Joint Engineering Laboratory for Fluid Transmission System Technology, Zhejiang Sci-Tech University, Hangzhou, Zhejiang 310018, China

²ZheJiangShangfeng Special Blower Industrial .co Ltd, Shaoxing, China

[†]Corresponding Author Email: yikunwei@zstu.edu.cn

(Received April 2, 2021; accepted December 27, 2021)

ABSTRACT

Numerical simulation was used to investigate the effect of an inclined volute tongue on the complex flow characteristics and the aerodynamic performance of multi-blade centrifugal fans. We focused on the effects of the clearance, the inclination angle and the volute tongue's on controlling the centrifugal fan's internal flow characteristics and aerodynamic performance. The results showed that the volute tongue's reasonable clearance ratio and the inclined volute tongue design were beneficial to improving the flow pattern around the volute tongue and volute outlet of the centrifugal fan, as well as reducing the local flow loss. It is of great significance to increase the centrifugal fan's static pressure and related efficiency by increasing the radius and inclination angle of the volute tongue. Due to the reduced of vortex, the local flow loss was reduced. Numerical results indicated that model C's static pressure rose to 12.5Pa, and the related static-pressure efficiency of to 3.8% compared with the reference geometry due to the reduced of flow loss.

Keywords: Centrifugal fan; Inclined volute tongue; Vortex structure; Dimensionless gap ratio; Flow loss

NOMENCLATURE

B	width of the volute	r	radius of volute tongue
b	width of the impeller	Z	blade numbers
D1	impeller inner diameter	β_1	inlet angle of the blade
D2	impeller outer diameter	β_2	outlet angle of the blade
n	rotational frequency of impeller	δ	thickness of the blade,
Qn	flow rate		

1. INTRODUCTION

The market demand for centrifugal fans gradually increases with the continuous development of the world industry. The centrifugal fan is a driven fluid-machinery, which depends on the input mechanical energy to improve the gas pressure and exhaust the gas (Cai *et al.* 2010; Van 2009, Chen *et al.* 2010). As an essential category of universal machinery, a centrifugal fan is widely used in world economy and social life. With the increasing importance of environmental protection and energy conservation, centrifugal fan's high efficiency is paid more attention. Reducing fan operation's energy consumption and increasing fan efficiency play a significant role in electricity and related-energy savings (Kind and Tobin 1990; Khelladi *et al.* 2008; Lin and Huang 2002). The multi-blade centrifugal

fan has been applied to industries. The multi-blade centrifugal fan is widely used in ventilation systems and air conditioning equipment (Ballesteros-Tajadura *et al.* 2006). Generally, centrifugal fan has the characteristics of high pressure and low efficiency, while axial fan has the characteristics of high flow and low pressure (Chen *et al.* 2020).

The impeller of a multi-blade centrifugal fan freely rotates in a volute (Zhang *et al.* 2006; Xu *et al.* 2005; Sun *et al.* 2009;Liu *et al.*2009).The volute geometry plays a significant role in the aerodynamic performance of the fan. The severe impact of airflow around the volute tongue and impeller outlet complicates the flow in the volute tongue area (Jadhav and Patil 2016). Patil *et al.* (2018) studied the effects of volute tongue inclination angle, volute tongue gap, and volute tongue installation position on the fan's

aerodynamic performance and noise characteristics. Patil *et al.* (2018) argued that the volute tongue clearance has a significant effect on the performance of centrifugal blower and aerodynamic performance of fan increases with the decrease of volute tongue clearances. The experiment presents the influence of the volute tongue modification on the fan's performance (Ting and Gang 2012; Wang *et al.* 2018). Suhrmann *et al.* (2012) studied the influence of the geometry of the volute tongue on the local flow characteristics of the fan. The influence of the volute tongue radius on the aerodynamic performance is studied experimentally and numerically, and obtained a series of suggestions for the modification of volute tongue. Numerical results are compared with the experimental results to analyze the volute tongue's internal flow characteristics in this paper. The accuracy of prediction and quantification are evaluated qualitatively, affecting the centrifugal fan's aerodynamic performance (Ballesteros *et al.* 2008, Velarde-Suárez *et al.* 2008; Xiong *et al.* 2018; Wu *et al.* 2020).

The change of the volute tongue gap is realized by increasing the distance between impeller and volute tongue, which improves fan's performance. Increasing the gap between the volute tongue and the impeller can make the blade leave the impeller boundary and reduce the volute's uneven flow, which improves centrifugal fan's performance. A significant change in pressure occurs near the tongue area of a large volute. With the increased distance from the tongue to impeller's external diameter, the pressure decreases gradually. The volute tongue's effect on the circumferential pressure distribution decreases with the increased distance from the volute tongue area to the impeller's external diameter (Zhang *et al.* 2016). The blocking effect decreases with the increased of the radial clearance, the difference between flow pattern and return flow increases with the increasing radial clearance. Therefore, the centrifugal fan's performance is greatly affected by the volute tongue's position (Yang *et al.* 2019).

Wei *et al.* (2020) and Darvish *et al.* (2014) studied the effects of the stepped volute tongue on internal complex flow, aerodynamics performance and noise control, and optimization of a forward multi-blade centrifugal fan. The tonal noise generation of the fan can be controlled by arranging cut-off and designing stepped tongues. Through computational fluid dynamics (CFD), Lun *et al.* (2019) and Li *et al.* (2020) argued that the inclined volute tongue affects aerodynamics performance and flow structure near the volute outlet and the volute tongue of the centrifugal fan, with detailed improvement suggestions proposed. Lee (2010) designed the CFD numerical simulation, and compared the impeller's whole flow field with/without gap and volute effect. In the preparation stage of numerical simulation, they discussed the uncertainty of numerical simulation and argued that fan's clearance flow affected the aerodynamic performance of the centrifugal fan. Mesh accuracy and turbulence models affect the

numerical calculation. Wolfe *et al.* (2015) introduced the experimental uncertainties to study the low-speed centrifugal fan's performance prediction model, and established a general model of performance trend diagram of double outlet centrifugal fan, which used the experimental data of vaneless diffuser turbocharger to draw the performance diagram of compressor with tip velocity Mach number of 0.4 ~ 2. Ballesteros *et al.* (2008) studied the factors that affecting the results of numerical simulation and experiment. The experiment's external conditions, such as temperature, atmospheric pressure, and voltage fluctuation, may cause uncertainties in the experiment. Some researchers (Zhou *et al.* 2021; Yang 2018; Ning *et al.* 2010) simulated centrifugal fans by CFD software. The centrifugal fans with different structures are simulated, and obtained the centrifugal fan with optimized performance. In this process, the specific simulation methods, such as mesh generation and boundary condition setting, are studied, and the simulation results and experimental data are compared to verify the reliability of the simulation method.

Based on the above discussions, changing the volute tongue's angle can improve the aerodynamic performance and the application of the fan. The present studies focus on the impact of increasing the volute-tongue clearance and its radius on the complex internal flow and aerodynamic performance of the centrifugal fan. Volute tongue clearance and radius are designed aerodynamic performance of the centrifugal fan. The Q-criterion is employed to identify vertical flow structures and high loss areas within the flow by which the influence of volute tongue clearance and tongue radius on the volute is studied, and the optimal solution for improving the performance of this fan is represented. The results of this paper should be applied to other centrifugal fans, optimizing the aerodynamic performance of a single impeller centrifugal fan with 60 forward blades.

Section 2 introduces the detailed parameters of the reference single-inlet multi-blade centrifugal fan. After that, the detailed fluid dynamics equations of internal flow are presented in section 3. Section 4 discusses the detailed experimental device and aerodynamic performance measure for single inlet centrifugal fans. Then, Section 5 presents various detailed internal flow characteristics and aerodynamic performance of four fan models. Section 6 gives the conclusion.

2.1. Parameters of original fan and modification of inclined volute tongue Parameters of Multi-blade Centrifugal Fans

As shown in Fig. 1, the multi-blade fan with a single inlet mainly includes a volute, a collector, a volute tongue, and an impeller with 60 forward blades. Table 1 presents the main parameters.

2.2 Geometries of inclining volute tongue and modification method

The volute tongue region's flow is very complicated due to the impeller outlet flow and volute tongue's

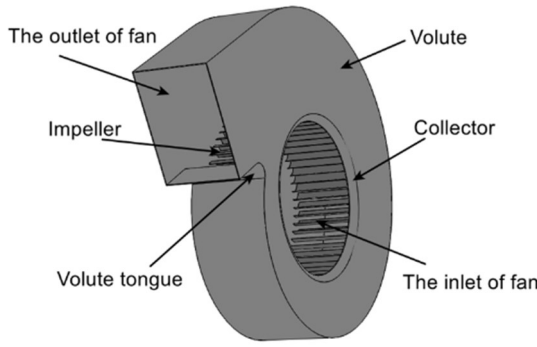


Fig. 1. Main structure of the referenced centrifugal fan.

Table 1 Parameters of the reference model

Parameters of the referenced fan	Sizes
Flow rate, Qn	845 (m ³ /h)
Rotational frequency of the impeller, n	750 (rpm)
Impeller's outer diameter, D ₂	280 (mm)
Impeller's inner diameter, D ₁	243 (mm)
Width of the volute, B	120 (mm)
Width of the impeller, b	100 (mm)
Inlet angle of the blade, β ₁	67.9 (°)
Outlet angle of the blade, β ₂	163.7 (°)
Thickness of the blade, δ	0.4 (mm)
Blade numbers, Z	60
Radius of volute tongue, r	17 (mm)
dimensionless gap ratio(Δt/d ₂)	0.084

mutual impact. The influence of the volute tongue dominates the aerodynamic performance and noise characteristics of the fan. The small changes of the volute tongue geometry and installation spacing significantly affect the fan's performance and noise. Therefore, the modification of the volute tongue can improve the flow condition and reduce the noise.

The volute tongue's inclination shows that the volute tongue's clearance and radius gradually increase from the disk side to the wheel-cover side, which reduces the dynamic and static interference of the wheel-cover side. On the other hand, the volute tongue's inclination also demonstrates that the interaction between the disk side and the wheel-cover side produces a specific phase difference. Therefore, several inclined volute tongues are redesigned from the air inlet to the rear panel of the fan to reduce the periodic interaction between the volute tongue and air flow caused by rotating impeller and improve the centrifugal fan's aerodynamic performance. The work focuses on three parameters for modifying the inclined volute tongue.

Figure 2 shows the sketch of several critical parameters for the modified centrifugal fan. In Fig. 2(a) and (b), the volute tongue's angle is adjusted by changing the volute tongue's radius on the back cover of the volute. Symbol θ denotes the angle between the central line of the modified geometry and the original geometry and its projection line. The tilt direction is raised from the volute's front cover plate to the rear cover plate. Figure 2(c) shows that Δt is the minimum distance from the volute tongue to the impeller's outer diameter D₂. The dimensionless clearance ratio introduced above plays a significant role in the aerodynamic performance and aerodynamic noise characteristics of a multi-blade centrifugal fan. Figure 2(d) shows the specific location of r₁ and r₂. r₁ is close to the volute front shroud, and r₂ is close to the volute's outlet side. B.E.K is used to deduce the formula of the inclined angle of the volute tongue of the centrifugal fan (Wang *et al.* 2021) :

$$\theta = \arccos \frac{(t + \Delta x) + b\sqrt{(t + \Delta x)^2 + b^2 - d^2}}{(t + \Delta x)^2 + b^2} \quad (1)$$

where t is the blade spacing at the impeller outlet; Δx the aerodynamic wake parameter; d the arc diameter of the volute tongue; b the volute tongue's width.

θ_{Δt} is considered the inclination angle of the volute tongue, and a correction value Δθ = 4° - 6° is added in the volute tongue's actual inclination angle. The angle of inclination is θ = θ_{Δt} + Δθ. The formula for calculating the inclination angle of the volute tongue is given by Cassell as (Heo *et al.* 2014),

$$\theta = \arctg \frac{b}{t - 2r} \quad (2)$$

where t is the blade row distance at the impeller outlet; r the volute tongue radius; b the width of the impeller outlet. In the work, the volute tongue's inclination angle is calculated as 15.34° by Formula (1) and 14.02° is implemented by Formula (2). Therefore, when the volute tongue's radius remains unchanged, the volute tongue's inclination angle is selected as 14.68° of model A.

The volute tongue radius r₂=23mm for model B and r₂=30mm for model C are implemented in the work to study the influence of volute tongue radius (the area impacted by airflow) on the aerodynamic performance of the centrifugal fan. The centrifugal fan's aerodynamic performance can be improved by increasing the volute tongue's affected contact area.

The three models of modified fans (A, B, and C) have different volute tongue radius and volute tongue clearances. In Fig. 2(d), the type-A radius of the volute tongue remains unchanged (r₁ = r₂ = 17mm), but the volute tongue clearance gradually increases r₂. The type-B volute tongue's radius is from 17mm to 23mm and that of type-C volute tongue from 17 to 30mm. Type-B and -C models vary in clearance and inclined angle. The dimensionless clearance ratios (Δt/D₂) of types A, B, and C are 0.069, 0.091, and 0.094, respectively.

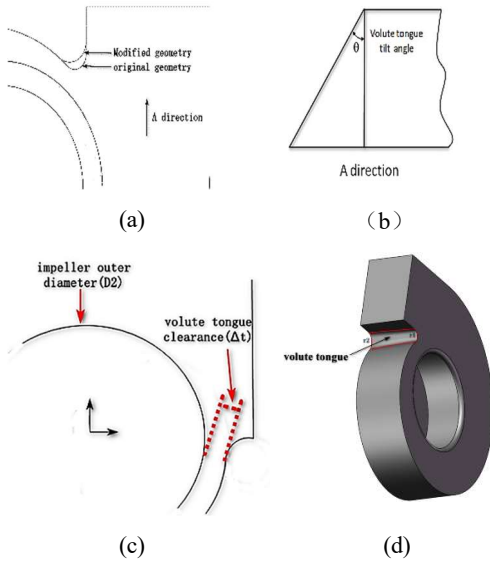


Fig. 2. Definition of volute tongue parameters.

Table 2 Key parameters of original and modified models with the inclined volute tongue

	Original	Model A	Model B	Model C
r1 (mm)	17	17	17	17
r2 (mm)	17	17	23	30
theta (degree)	0	14.68	3.96	7.87
Delta t/D2	0.08375	0.069	0.0909	0.0937

3. Numerical and experimental approaches

3.1 Numerical methods

The fluid dynamics with the turbulence model is implemented to simulate internal flow in the centrifugal fan. The solution of turbulence is based on the Navier-Stokes (N-S) equation in traditional computational fluid dynamics. The Reynolds average method can be used to average the time of the unsteady N-S equation and obtain the average quantity of an engineering problem. The dynamic equation and momentum conservation equation of flow is given as,

$$\frac{\partial(\rho u_i)}{\partial x_i} = 0 \quad (3)$$

$$\frac{\partial(\rho u_i u_j)}{\partial x_j} = f_i - \frac{\partial P^*}{\partial x_i} + \frac{\partial}{\partial x_j} \left[u_e \left(\frac{\partial u_i}{\partial x_j} + \frac{\partial u_j}{\partial x_i} \right) \right] \quad (4)$$

where ρ is fluid density; x_i and x_j are the components x , y and z in the Cartesian coordinate system in three directions; μ_i and μ are the average relative velocity components u , v and w ; P^* the reduced pressure; f_i the volume force component; μ_e the efficient viscosity coefficient, and $\mu_e = \mu + \mu_t$; μ molecular viscosity coefficient; μ_t the turbulent vortex viscosity

coefficient, respectively. The Rng k- ϵ kinetic energy k equation and ϵ diffusion equation of turbulence model is (Gun *et al.* 2016) :

$$\begin{aligned} & \frac{\partial}{\partial t}(\rho k) + \frac{\partial}{\partial x_i}(\rho k u_i) \\ & = \frac{\partial}{\partial x_j}(\alpha_k u_{eff} \frac{\partial k}{\partial x_j}) + G_k + G_b - \rho \epsilon - Y_M + S_k \end{aligned} \quad (5)$$

$$\begin{aligned} & \frac{\partial}{\partial t}(\rho \epsilon) + \frac{\partial}{\partial x_i}(\rho \epsilon u_i) = \frac{\partial}{\partial x_j}(\alpha_\epsilon u_{eff} \frac{\partial \epsilon}{\partial x_j}) + \\ & C_{1\epsilon} \frac{\epsilon}{k} (G_k + C_{3\epsilon} + G_b) - C_{2\epsilon} \rho \frac{\epsilon^2}{k} - R_\epsilon + S_\epsilon \end{aligned} \quad (6)$$

where G_k represents the turbulent kinetic energy generated by the laminar velocity gradient; G_b the turbulent kinetic energy produced by buoyancy; Y_M the wave generated by the diffusion of transition in compressible turbulence; $C_{1\epsilon}$, $C_{2\epsilon}$ and $C_{3\epsilon}$ are constant number, α_k and α_ϵ are the turbulence Prandtl numbers of the k and ϵ equations, respectively.

3.2 Grid of Multi-blade Centrifugal Fan

Generally, the quality of the grid plays a significant effect in the numerical calculation of centrifugal fans. The grid tool of ICEM is devoted to discretize the flow area into grids, and the hexahedral structured grids are used for the relatively regular geometry. A boundary layer appears near the solid wall, and the flow of fluid produces a velocity gradient. The velocity gradient changes significantly in the boundary layer, so the grids near the wall and the blade surface are used to capture the varieties. The impeller and volute tongue are the key areas for analysis where the grid density is larger than other regions. The grids of all computational area are refined in the boundary regions. The impeller and volute tongue have a slightly larger refinement.

3.3. Computational Domain of Multi-blade Centrifugal Fans

This section will introduce the computational geometry model of centrifugal fans. Figure 4 shows the geometric model of the fluid domain. The centrifugal fan model's computational domain consists of semicircular inlet region, impeller region, volute region and outlet region to obtain its performance and simulate its internal flow characteristics. According to the fan's actual operation and experiment, the section outlet is set, and the model has been simplified. All numerical simulations of single impeller centrifugal fans with 60 forward blades are carried out in the work.

This section describes the boundary conditions for all numerical simulations, where the air density is 1.225 kg/m^3 , and the viscosity is $1.7894 \times 10^{-5} \text{ kg/(m*s)}$. Since the computational domain is divided into the rotating domain and other stationary domain of the impeller, the whole domain of the impeller is regarded as the rotation domain, with the given speed is 800r/min. The multi-reference system is implemented to set the rotation domain, and the rest of the wall is fixed

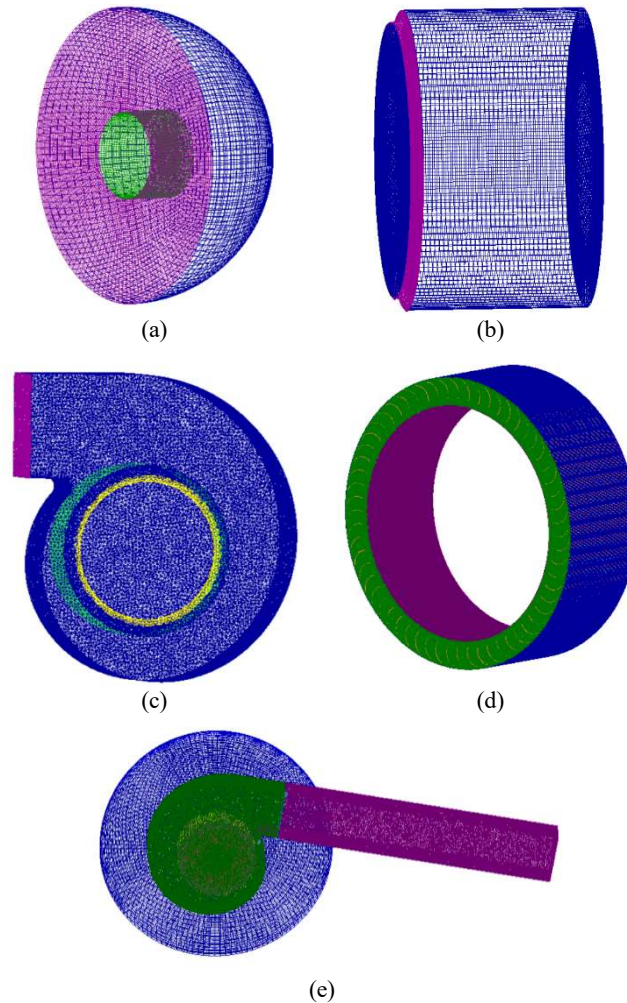


Fig. 3. Computational domain grid and the whole grid.

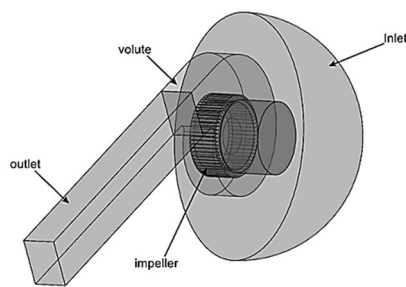


Fig. 4. Computational domain of the original centrifugal fan.

without slip. The static outlet pressure is consistent with the atmospheric pressure. The inlet boundary is defined as the mass flow inlet, and the outlet boundary is the pressure outlet boundary in the whole calculation domain.

The numerical simulation of the steady flow was performed in the work. Five interfaces were implemented in our numerical simulations, namely the interface between the inlet and gas skirt, the

interface between gas skirt and hub, the interface between hub and impeller, the interface between impeller and volute, and the interface between volute and outlet. The interface mode was set for the general connection. The impeller and volute were the interface between rotating parts and static parts, and the interface type was set as the frozen rotor model. The value of y^+ was 33 in numerical simulation. The wall treatment was enhanced as a near-wall treatment to improve the boundary layer problem's computational accuracy. As a less refined mesh was performed, the effect of enhanced wall treatment is remarkable. The maximum residual error of all the numerical simulation results is less than 1×10^{-3} in this work, the flow rate is almost equal in the inlet and outlet, and the error of the flow rate is less than 0.5% in the inlet and outlet. Therefore, the numerical simulation results are considered to be convergent.

3.4. Grid independence verification

Five groups of grids are used to verify the grid independence, thus determining the numerical simulation's final grid scheme. All numerical simulations were carried out under the same conditions. Figure 5 shows the relationship between grid number and fan pressure. It can be seen from

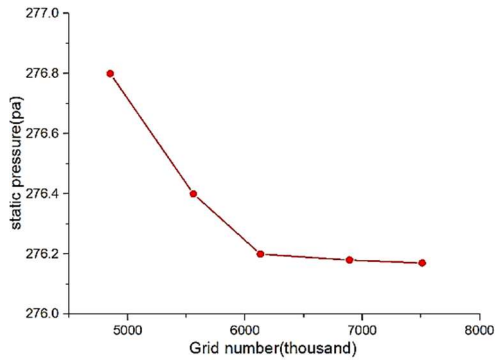


Fig. 5. Static pressure of different grids at design condition (Q_n).

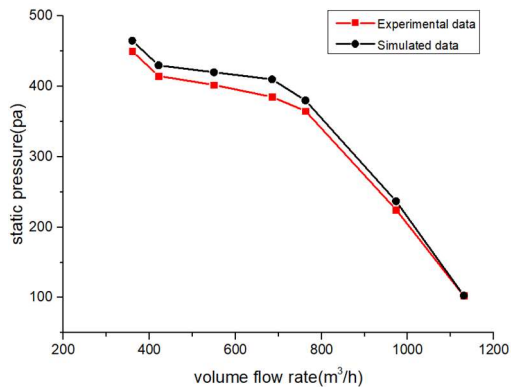


Fig. 6. Static pressure comparison between numerical and experimental results in different volume flow rates.

the plotline that when the grid number is 6 million, the number of grids is independent of the calculation results, and the numerical results can achieve an ideal convergence effect.

3.5. Verification of numerical simulation method

The static pressure of a centrifugal fan was taken as the reference to verify the numerical method's accuracy. Figure 6 illustrates the static pressure comparison between experimental and numerical results at different flow conditions. Table 3 shows the static pressure values of the experimental and numerical simulation in seven flow rates. The static pressure of experimental and numerical results gradually decreases with the increasing flow rate (from 345.3 m³/h to 1138.6 m³/h). The numerical results are well consistent with the experimental test's static pressure trend. The maximum static pressure difference between experimental results and numerical results is 7.6Pa, and the error is less than 2%, which meets the error requirements. This also demonstrates that the numerical method is reliable in the work. It can be used for the next step of flow characteristics analysis of centrifugal fans.

4. Experiments on Aerodynamic Performance

This experiment was used to obtain the centrifugal fan's performance and learn the determination method of the characteristic curve of the centrifugal

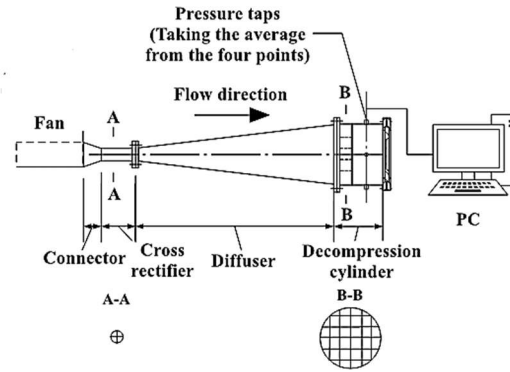


Fig. 7. Centrifugal fan performance test installation.

fan. In general, the multi-blade centrifugal fan's test method was mainly applied to the measurement of external macro performance, while the experimental measurement of the internal flow field was not realized. The test equipment of the centrifugal fan performance is introduced in the following section.

Figure 7 shows the experimental device for aerodynamic performance. The air performance test device is connected with the test fan's outlet of the test fan through a connector, and the other end of the air performance test device is connected to a cross rectifier, a diffuser, an air pressure reducing cylinder, and a computer with the data receiver. The pressure reducing cylinder at the fan performance test outlet is connected with four adjustable orifice plates, and the flow regulation is realized by replacing orifice plates of different diameters. The static pressure is measured by four pressure taps located on the cylinder wall.

The performance test rig of the centrifugal fan is used to measure the pressure and speed parameters. The fan's performance is expressed by total pressure drop (Pa) - volume flow rate (m^3/h). Air volume (Q_v) is the volume of air discharged from the fan outlet per unit time, which can be controlled by the throttle. The air volume is measured utilizing a pitot tube. Pitot tube is a tubular device composed of a cylindrical flow head which is perpendicular to the supporting rod. The device has some static pressure holes around the side wall and a full pressure hole facing the flow at the top. The total pressure hole feels the average pressure near the stagnation point, which is slightly lower than the total pressure. The static pressure felt by the static pressure hole also has a certain error. For pitot tubes of any size, when the medium flows are measured through the detection rod, it will form a flow around and change the streamline, so as to

change the local pressure Sun *et al.* (2007). In addition, the flow around the downstream vertical detection rod will have an impact on the accuracy of static pressure measurement. Therefore, a correction coefficient ξ should be added when the flow velocity is calculated (Zhou *et al.* 2017). The calibration value is 1.02 in this experiment.

Two ducts are used one goes deep into the center of the ventilation duct, and measures the maximum wind pressure P_1 at the shaft (pipe) center, and the other measures the static pressure P_2 on the pipe wall through:

$$v = \sqrt{2(p_1 - p_2) / \rho} \quad (7)$$

The maximum point velocity is calculated at the pipe axis, and then the air volume is calculated by multiplying the cross-sectional area of the pipe according to the relationship between the maximum velocity and the average velocity. Dynamic pressure of the air flow is (f_1-f_2) in Equation (7), which can be calculated from the air volume Q measured by the pilot tube.

The actual effective energy of the air delivered from the fan per unit time is called the total- pressure effective efficiency of the fan:

$$N_e = \frac{P_T Q_v}{1000} \quad (8)$$

where N_e represents the effective power (kW); P_T the total pressure (Pa); Q_v the volume flow rate (m³/s).

The energy transmitted by the prime mover to the fan shaft in unit time is called the fan's shaft power. It is also known as the input power written as :

$$N_s = N_i + \Delta N_m \quad (9)$$

Where N_s represents the input power (kW); N_i the internal power(kW); ΔN_m the mechanical loss of power(kW), respectively. The efficiency of the fan (η) can be expressed as:

$$\eta = \frac{N_e}{N_s} \quad (10)$$

5. RESULTS AND DISCUSSIONS

5.1 Effect of inclining volute tongue on static pressure

Figure 8 illustrates the location of the planes employed to verify the flow behavior in different operating conditions. The middle disc position is $Z = 0$ mm, and three planes are taken along the positive direction of the Z-axis ($Z = 15, 30$ mm and 45 mm). The internal flow field is analyzed by giving the parameters on three planes. In the following subsection, the baseline model's static pressure fields and the three modified models are analyzed through numerical simulation in the designed flow rate ($Q_n=845\text{m}^3/\text{h}$).

Figure 9 shows the distribution of static pressures at $Z=15, 30$ mm and 5 mm. The difference in static pressure distribution near the volute tongue is one of

the key factors to reveal the centrifugal fan's aerodynamic performance due to the periodic interaction between the volute tongue and airflow caused by the rotating impeller. The high difference of static pressure distribution near the volute tongue produces a strong backflow at the volute outlet, reducing the aerodynamic performance of centrifugal fan.

In Fig. 9, a large difference in static pressure distribution near the baseline model's volute tongue can be observed in all three sections. The relatively low difference of static pressure distribution mainly occurs near the volute tongue of model A compared to that of the baseline model. The difference of static pressure distribution slightly decreases near model B and C near the volute tongue. Moreover, model C's static pressure distribution is uniform near the volute tongue, and the least difference distribution of the static pressure for model A is captured at the volute tongue. The loss of aerodynamic flow due to the difference of static pressures for models A, B and C near the volute tongue and at $Z=15$ mm is mildly lower than that of the baseline model. In general, the aerodynamic flow loss mainly occurs at the high the difference of static pressures, and velocity. Figure 9 (i) shows the static pressure distribution baseline model and model A at $Z = 15$ mm plane. As Fig. 1, it can be seen from the black box that the high pressure distribution area of model A is significantly less than that of the baseline model, as well as Model B and Model C.

For the section at $Z=30$ mm, the difference of static-pressure distribution slightly decreases near the volute tongue of the models A, B and C. Especially, the lowest static-pressure difference of models A and C appears near the volute tongue, which indicates that the models A and model C have the lowest loss.

For the section at $Z=45$ mm section, the lowest difference of static-pressure distribution for model C appears near the fan's volute tongue. The distribution of static-pressure difference for models A,B and C near the volute tongue decreases compared to that of the baseline model in the sections at $Z=15, 30$ and 45 mm. The lowest difference of static pressure distribution for model C appears near the fan's volute tongue, which produces the low backflow phenomenon with high aerodynamic performance

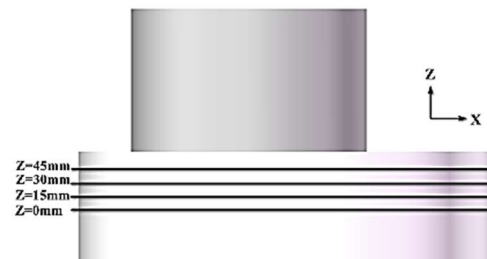


Fig. 8. Planes in different positions.

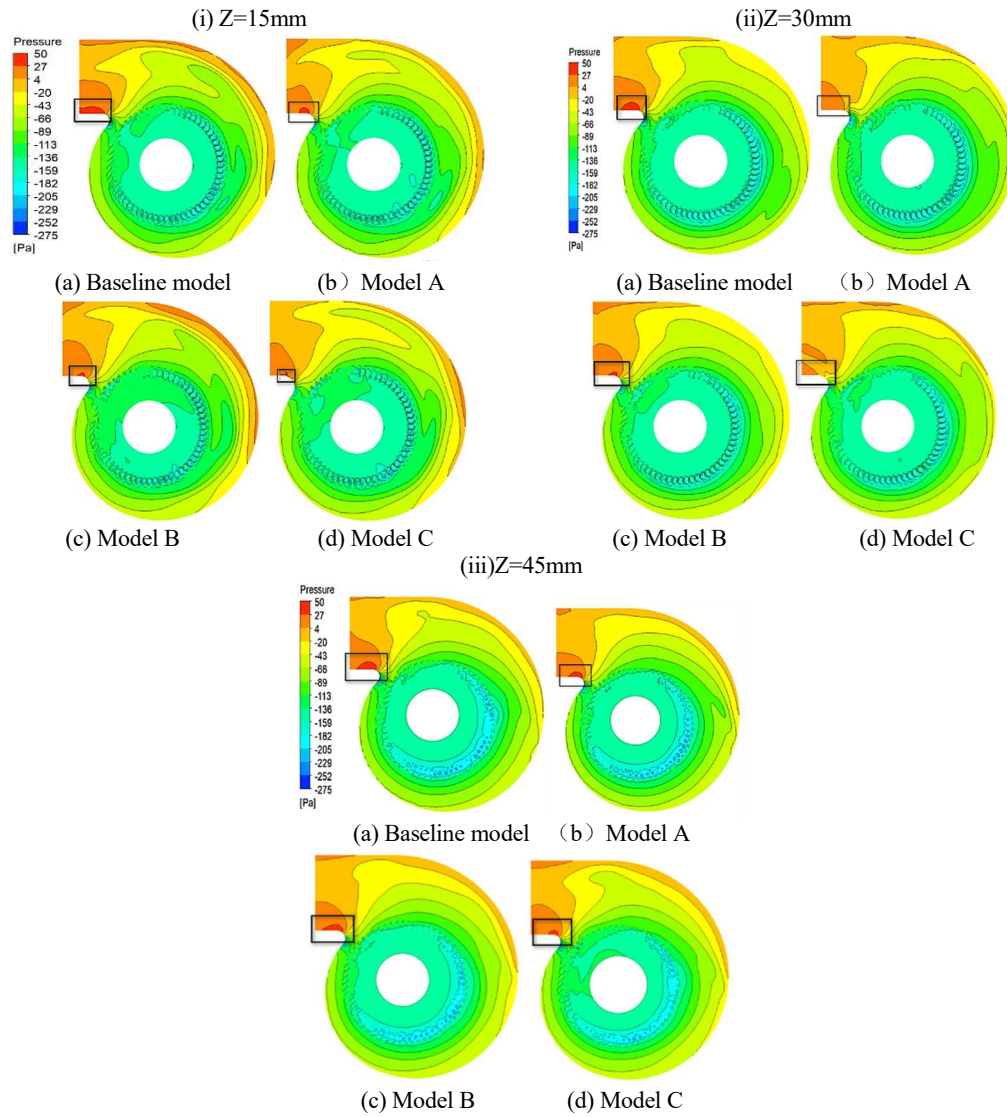


Fig. 9. Distribution of static pressures in different sections (Q_n).

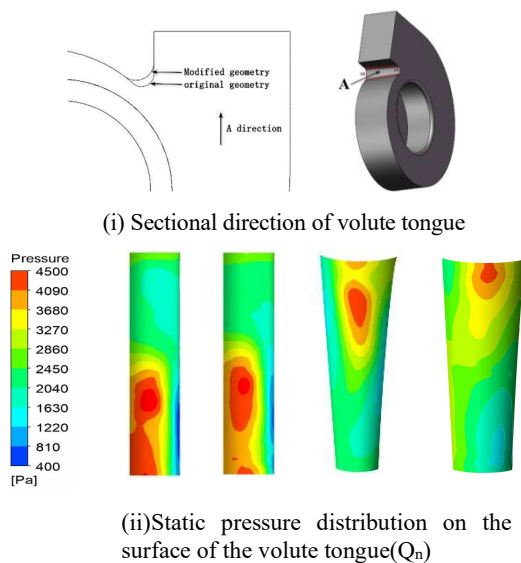


Fig. 10. Volute tongue surface direction and pressure distribution.

Figure 10 shows the volute tongue surface direction and pressure distribution in the designed flow rate. Figure 10 (i) describes the schematic diagram of observation direction of volute tongue. Besides, the four models' high-pressure areas are distributed on the top of the volute tongue. As can be seen from Fig. 10(ii), compared with the baseline model, the increasing volute tongue clearance reduces the high-pressure area on the surface of volute tongue surface. Compared with the baseline model, models B and C show that with the increased volute tongue's inclination angle, the maximum pressure value decreases significantly, and the area occupied by the high-pressure area decreases gradually, owing to the increased inclination. The distance between the volute tongue and the impeller outlet increases, and the impact between the blade outlet and the top of the volute tongue is weakened. Furthermore, the low pressure area gradually reduces, and its value also enlarges with the increased inclination angle. Thus, the pressure difference on the top of the volute tongue reduces, which improves the fluidity and vortex structure of the volute tongue. The highest

pressure area of the baseline model and model A is distributed in the middle and lower position of the top of the volute tongue. with the increased of volute tongue inclination angle(model B and model C), this area gradually moves to the top of the volute tongue close to the rear cover plate side of the volute, because after the volute tongue inclined, the airflow impact at the impeller outlet is slightly offset. However, it deviates with the increased of the inclination angle of the tongue. Meanwhile, the static pressure distribution on the surface of volute tongue of all models in Fig. 10 further shows that the static pressure distribution of models A, B and C is less than that of the baseline model. Therefore, it is concluded that near the volute tongue, the flow loss of each improved model is lower than that of the baseline model, and the performance of the model is optimized.

5.2 Effect of the inclined tongue on the structure of vortex

The Q-criterion is used to provide insight into the flow field’s local flow loss (Sistek 2015; Wu *et al.* 2013). In the work, two dimensional Q value in the z-direction section and the three-dimensional Q value of the internal flow are investigated, respectively.

$$Q = \frac{1}{2}(\Omega_y \Omega_y - S_{ij} S_{ij}) \tag{11}$$

$$\Omega_y = \frac{1}{2} \left(\frac{\partial u_i}{\partial x_j} - \frac{\partial u_j}{\partial x_i} \right) = \frac{1}{2} [\nabla_u - (\nabla_u)^T] \tag{12}$$

$$S_{ij} = \frac{1}{2} \left(\frac{\partial u_i}{\partial x_j} + \frac{\partial u_j}{\partial x_i} \right) = \frac{1}{2} [\nabla_u + (\nabla_u)^T] \tag{13}$$

Figure 11 shows the Q value distribution at Z=15, 30mm and 45mm for the different models. Several Q-value distributions for all four models are shown on the impeller’s volute’s outer wall and the inner surface.

Figure 11 shows the distribution of Q values of the modified models A, B and C is significantly lower than that of the reference model. The baseline model’s Q-value distribution is also higher than that of other models near the volute wall. From the view of the vortex structure’s morphological character, the baseline model’s vortex structure with a flat tongue is a single vortex core. However, when the volute tongue is inclined, the vortex structure is still a single vortex core, and the vortex scale reduces. It is worth mentioning that the Q-value distribution of model A is mainly distributed on the volute’s upper wall. However, models B and C are mainly distributed on the bottom wall. Overall, the Q-value distribution of all the modified models is reduced to some extent compared with the baseline model, and the lowest Q-value distribution appears in model C.

In the section at Z=30mm for the different models, all models Q values are mainly distributed on the outer wall of the volute and the inner surface of the impeller. The Q-value distribution of model B is higher than all other models near the wall of the volute. The Q-value distribution of all the modified models decreased to some extent compared with the

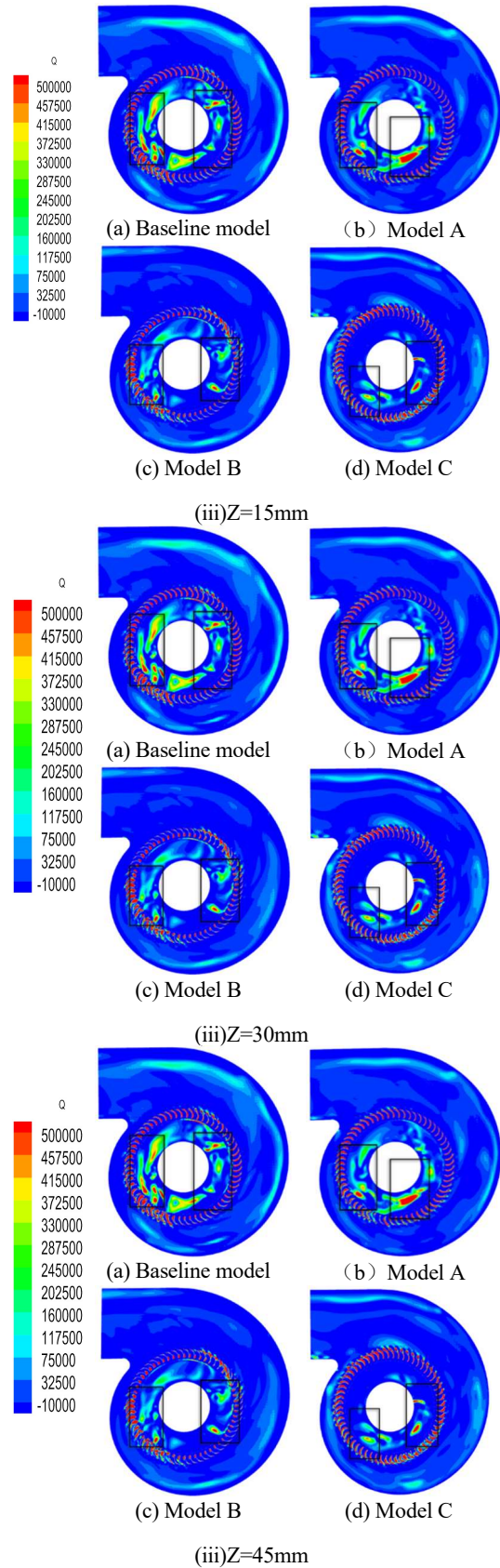


Fig. 11. Q value distribution in different sections(Qn).

baseline model, and the lowest Q-value distribution for model C appears in the internal flow of the

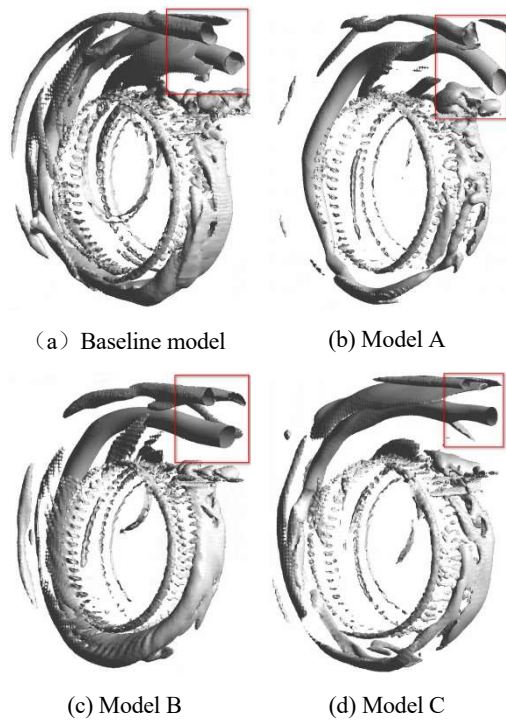


Fig. 12. Distribution of three-dimensional vortex structure in the volute domain.

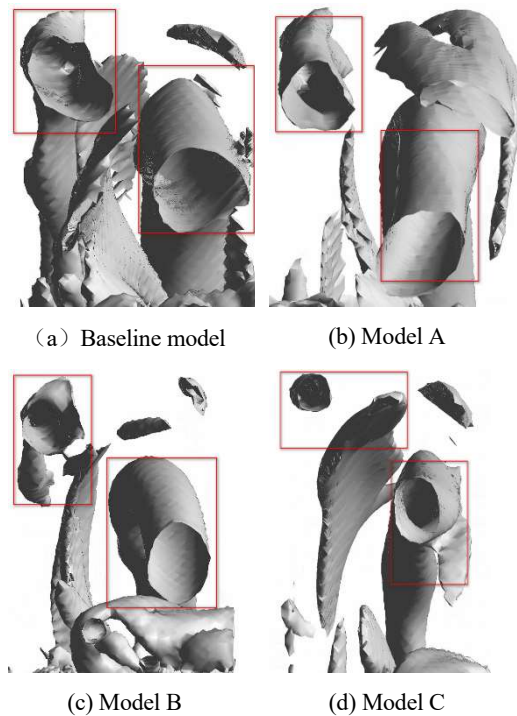


Fig. 13. Enlarged three-dimensional vortex structure at the volute outlet.

impeller, indicating that the local flow loss of model C is the least in all models in the sections at $Z=30\text{mm}$.

For the section at $Z=45\text{mm}$, the lowest Q -value for the model C appears in the impeller's internal flow at

the marked position. Moreover, the vortex structure is similar to the mentioned planes. The difference of the distribution of Q -value for the models A, model B and model C decreases compared to that of the baseline model in the sections at $Z=15, 30$ and 45mm . The lowest Q is obtained for model C in the internal flow of the impeller. In general, model C's local flow at different sections is less than that of other models.

The three-dimensional Q vortex iso-surface in the following section to further reveal the centrifugal fan's complex flow. Figure 12 illustrates the distribution of three-dimensional vortex structure in the volute domain. The Q vortex structure of the baseline model is roughly divided into two parts at the volute outlet. The Q vortex structure's distribution area in the left half of model A is similar to the reference model. However, the Q vortex structure's distribution area is lower than that of the reference model, while the Q vortex structure in the right half remains approximately the same.

Figure 13 describes the locally enlarged view of the three-dimensional vortex structure in the volute outlet area. The comparison between Baseline model and model B shows the overall vorticity of model B at the volute outlet is less than that of the baseline model at the same threshold, which indicates that the local flow loss of model B at the volute outlet is less than that of the baseline model. Therefore, the Q vortex isosurface distribution of the three modified models near the volute outlet is lower than that of the baseline model. The Q vortex iso-surface distribution area in the left half of model B decreases, while the Q vortex iso-surface in the right half decreases slightly. In the two parts of model C, the Q vortex iso-surface is significantly smaller than that of the reference model. The Q vortex iso-surface distribution of the three modified models near the volute outlet is lower than that of the baseline model. The least Q vortex iso-surfaces for model C appear in the outlet of the centrifugal fan volute.

The inclined volute tongue structure reduces the size of the vortex zone at the volute tongue on the motor side and non motor side, reduces the interaction between air flow and volute tongue, reduces the size of the vortex zone at the volute tongue, especially near the wind circle. Inclining the volute tongue will reduce the air velocity in the volute tongue area and the difference of static pressure distribution on the surface of the volute tongue. At the same time, it will reduce the local swirl in the volute tongue area. In sum, the above series of explanations demonstrate that the geometry of the inclined tongue causes such significant redistributions of vortices structure in a whole fan.

In general, the overwhelming majority part of air gas is transported out. However, part of the airflow continues to rotate periodically with the impeller in the centrifugal fan. Many factors may affect the aerodynamic performance of the fan. The internal flow characteristics play a pivotal role in the upstream area of fan volute tongue and the downstream fan volute tongue.

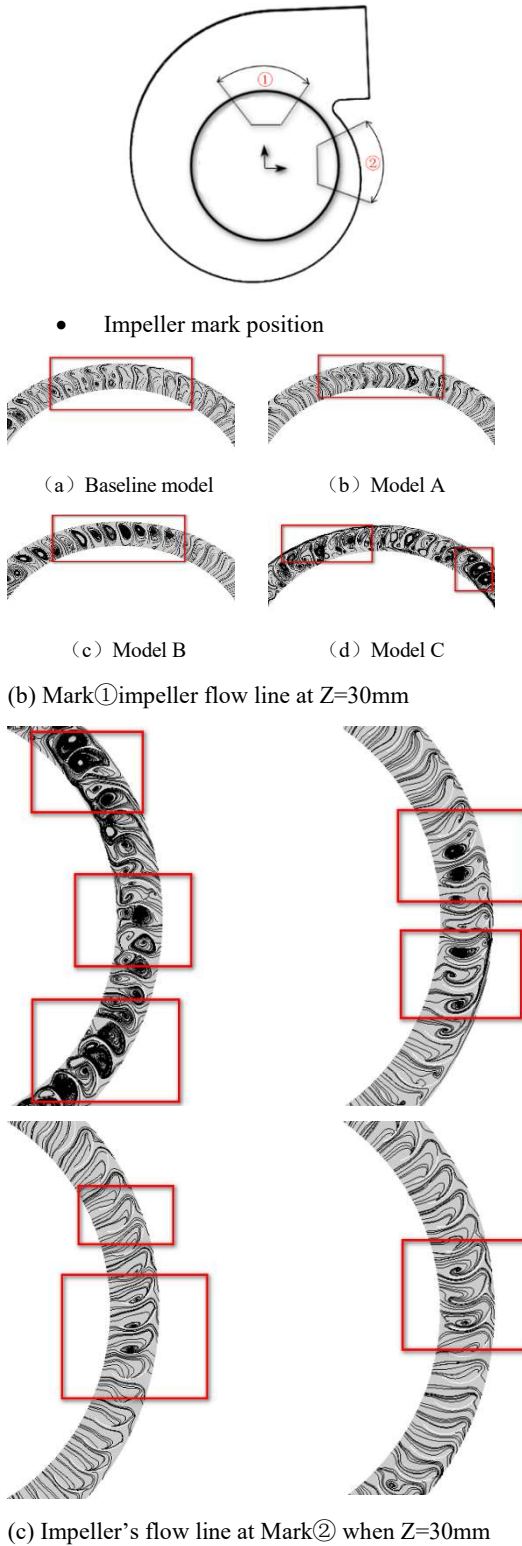


Fig. 14. Streamline distribution in blade channel at the marked position of the impeller (Q_n).

Figure 14 shows the streamline distribution in two marked positions of the impeller. The streamline distribution is drawn based on the velocity vector of secondary flow. In Fig. 14a, the upstream area of the fan volute tongue (channel 1) and downstream area

of the fan volute tongue occur in channel 2 of the impeller. As described in Fig. 14b, many small vortices for the reference model, and models A, B and C occur in the channel 1 of the impeller. The number of small-scale vortices of the baseline model and model A in channel 1 of the impeller is less than that of models B and C. In Fig. 14(c), a large number of small vortices for the baseline model appear in channel 2 of the impeller, and small scale vortices of models A, B and C in the channel 2 of the impeller are less than that of the reference model, indicating abundant air-flow for models A, B and C are almost transported.

The corresponding comparison in Fig. 14 demonstrates that the transported airflow for models A, B and C are almost more than that of the reference model, revealing that the aerodynamic performance of models A, B and C is higher than that of the reference model.

where k is the turbulent kinetic energy; u the average velocity; I the turbulence intensity. The large turbulence kinetic energy indicates the large turbulence fluctuation length and time scale, which measure turbulence's relative intensity. The place vortex mainly occurs in the place where the turbulence intensity is immense.

Figure 15 shows the turbulent kinetic energy distribution of the volute. The turbulent kinetic energy distribution near all the modified models' volute tongue is significantly lower than that of the baseline model. The low turbulent kinetic energy distribution of model C occurs near the fan's volute tongue compared to other models.

Turbulent intensity is the ratio of fluctuation standard deviation of the turbulence intensity to the average velocity,

$$k = \frac{2}{3}(u * I)^2 \quad (14)$$

5.3. Influence of inclined tongue on volute outlet X-velocity

Five heights are taken to show the velocity distribution at the volute outlet, demonstrating the flow characteristic of the volute outlet. Figure 16 displays the five sections of the volute outlet from bottom to top. The five height sections (5, 10, 30, 50 and 70%) are shown on the volutes' outlet surface to analyze the return area's flow characteristic on the outlet surface.

Figure 17 shows the velocity distributions on the five considered sections. The x-coordinate axis denotes the axial position, and the y-coordinate axis represents the volute outlet's vertical velocity. The backflow mainly occurs in the area below 50%H. Significantly, the backflow phenomenon gradually improves in the area below 30%H, which significantly influences the centrifugal fan's aerodynamic performance. Velocity perpendicular to the outlet plane of volute for models A, B and C is higher than that of the baseline model in the 5, 10, 30, and 50% height sections. However, the backflow mainly disappears in the 70%H section.

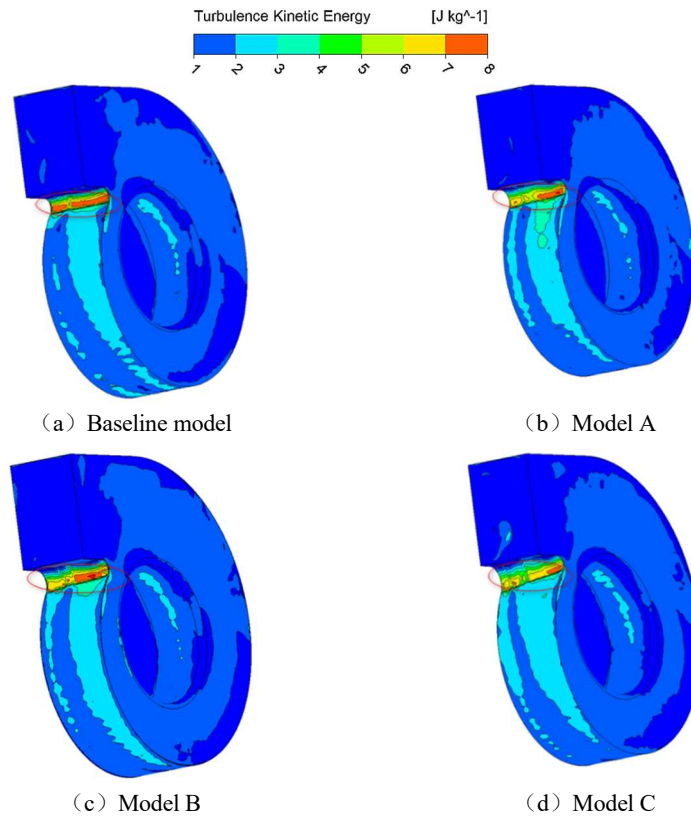


Fig. 15. Turbulent Kinetic Energy of volute (Q_n).

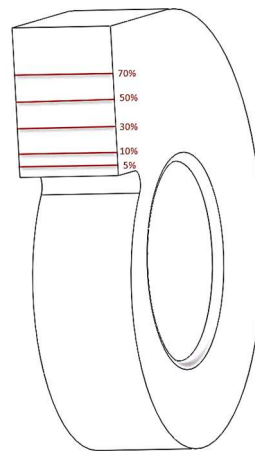


Fig. 16. Linear position of the volute outlet.

Due to the close distance to the outlet wall, two peaks of velocity occur in the region with low exit height. With the increasing exit height of all centrifugal fans, the axial distance between the two peaks gradually reduces. In the baseline model, the peaks eventually merge and reach a stable state in the region with high exit height. On the whole, obvious reflux appears on both sides of the volute outlet surface. In the whole exit surface of all centrifugal fans, the backflow zone mainly exists in the lower part, and the backflow zone gradually disappears with the increasing height of the exit surface.

Meanwhile, the inclined volute tongue structure

reduces the size of the vortex zone at the volute tongue on the motor side and non motor side, reduces the interaction between air flow and volute tongue, reduces the size of the vortex zone at the volute tongue, especially near the wind circle. Inclining the volute tongue will reduce the air velocity in the volute tongue area and the difference of static pressure distribution on the surface of the volute tongue. At the same time, it will reduce the local swirl in the volute tongue area. In sum, the above series of explanations demonstrate that the geometry of the inclined tongue causes such significant redistributions of vortices structure in a whole fan.

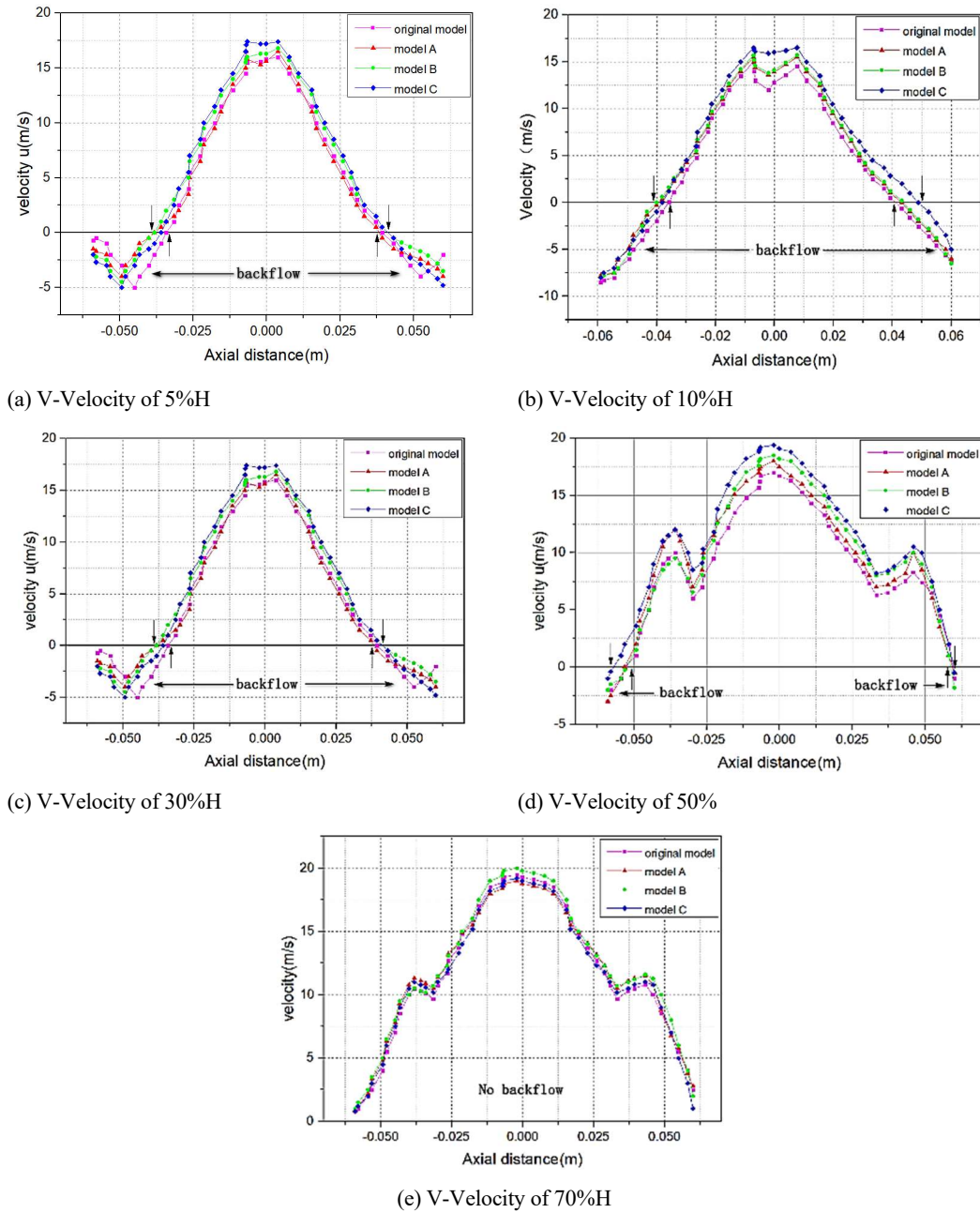


Fig. 17. Five sections velocity of the volute outlet along with the height.

5.4 Effect of the inclined volute tongue on performance

Figure 18 shows the baseline model's static pressure curves, and models A, B and C in different flow rates. The static pressure of model C in the whole flow range is significantly higher than that of the baseline model, while the pressure value of models B and C in the low and medium flow rates is slightly higher than that of the reference fan model. The pressure value of all models at the high flow has little difference. In the designed small flow rate, the static pressure values of models A, B and C are slightly higher than that of the baseline model. The static pressure of modified model A is 2.8 Pa higher than that of the baseline model, that of model B is higher

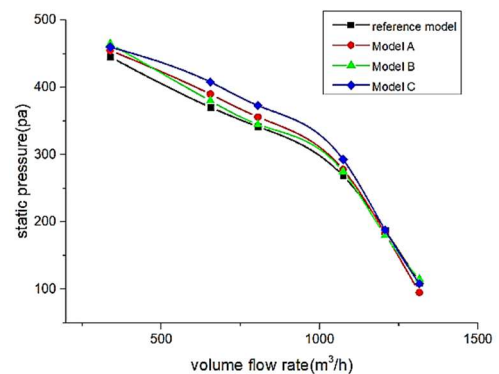


Fig. 18. Static pressure curve of the centrifugal fan.

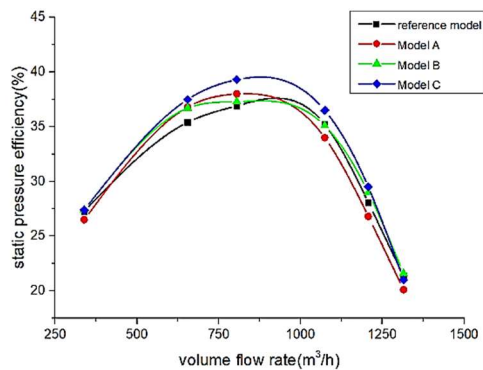


Fig. 19. Static pressure efficiency curve of the fan.

5.9 Pa high, model C rises as much as 12.5 Pa compared to that of the baseline model in designed flow rates. In a large flow rate, the four models' pressure values have little difference. By comparing the baseline model and model A, the fan's static-pressure value increases with the increased volute tongue clearance in a certain range. Compared to the baseline model's static pressure, and models B and C, the fan's static pressure value of fan increases with the increased of volute-tongue tilt angle.

Figure 19 illustrates an inclined volute tongue's effect on a centrifugal fan's static pressure efficiency, and static-pressure efficiency is the ratio of static pressure effective power and shaft power. The efficiency flow curve shows that the inclined volute tongue significantly affects the static-pressure efficiency. In the low flow rates, the efficiency of models A, B and C is higher than that of the baseline model, the efficiency value of model C is the highest in the designed flow rates, the efficiency of models A and B is slightly higher than that of the reference model. The improved static-pressure efficiency of models A and B rises as much as 1.2% compared to that of the reference model. The improved static pressure efficiency of model C rises as much as 3.8% compared to that of baseline model in the designed flow rates. In the high flow rates, the efficiency values of each model are similar. The flow value of the modified model's best efficiency point is lower than that of the baseline model due to the improved volute tongue structure and the reduced the area of the vortex region. Compared to the complex internal flow of several centrifugal fan models, model C has a better aerodynamic performance. The results demonstrate that the static-pressure efficiency is closely related to the internal vortex structure.

5. CONCLUSION

The work analyzed the effect of an inclined volute tongue on the fan's aerodynamic performance and the flow structure in the volute tongue area, as well as the impact of airflow on the volute tongue.

The increasing radius and the volute tongue's inclination angle reduced the static-pressure difference near the volute tongue. Besides, the turbulent kinetic energy distribution near the volute

tongue and the Q-value distribution of the impeller's internal flow were also related to the radius and the inclination angle. They could also control the vortex structure near the volute outlet and increase the volute outlet section's velocity perpendicular. The increasing radius and the volute tongue's inclination angle significantly increase the static pressure and the efficiency of the static pressure.

Compared with the baseline model in the designed flow rates, model A's static pressure rose as much as 2.8 Pa with a growth rate is 0.8%. Model B's static pressure rose as much as 5.9 Pa with a growth rate of 3.2%. The static pressure of model C rises as much as 12.3 Pa, and the growth rate of static pressure is 5.8%. Model A and B's static pressure efficiency rose as much as 1.2% compared to that of the baseline model. The static pressure efficiency of the model C rose as much as 3.8% compared to that of the baseline model in the designed flow rate.

In conclusion, the inclined volute tongue's design has the following advantages: improve the flow state near the volute tongue and volute outlet of centrifugal fan, prevent partial flow circulation, reducing adverse phenomena (including vortex and backflow), and enhancing the aerodynamic performance of the centrifugal fan. The 3D printing of the volute tongue surface of the models A, B and C will be accomplished. The aerodynamic performance and noise characteristics of the models A, B and C will be studied using experimental test, extending the application of integrated stoves.

ACKNOWLEDGEMENTS

This work was supported by National Natural Science Foundation of China (11872337, and 11902291), the Key Research and Development Program of Zhejiang Province (2020C04011) and Public Projects of Zhejiang Province (LGG21E0600, LGG20E060001), the development of three-dimensional detection for heads of pressure special equipment(20191203B74), and Natural Science Foundation Key Projects of Zhejiang Province (LZ22E060002).

REFERENCES

- Ballesteros, T. R., S. Velarde and C. J. P. Hurtado (2008). Noise Prediction of a Centrifugal Fan: Numerical Results and Experimental Validation. *Journal of Fluids Engineering*. 130(9), 253-257.
- Ballesteros-Tajadura, R., S. Velarde-SuaRez and J. P. Hurtado-Cruz (2006). Numerical Calculation of Pressure Fluctuations in the Volute of a Centrifugal Fan. *Journal of Fluids Engineering* 128(2), 359.
- Cai, J. C., D. T. Qi, F. A. Lu and X. F. Wen (2010). Study of the Tonal Casing Noise of a Centrifugal Fan at the Blade Passing Frequency. *Journal of Low Frequency, Vibration & Active Control* 29(4), 253-266.
- Chen, W., M. Wang, K. Mai, H. Li and N. Liu

- (2020). Structure design of low-frequency broadband sound-absorbing volute for a multi-blade centrifugal fan. *Applied Acoustics*, 165.
- Chen, Y. (2010). *Optimization of Aerodynamic Performance and Noise Control on a Forward Curved Centrifugal Fan*. Huazhong University of Science and Technology. Wuhan, China.
- Darvish, M., B. Tietjen, D. Beck and S. Frank (2014). Tonal Noise Reduction in a Radial Fan With Forward-Curved Blades. Proceedings of the ASME Turbo Expo 2014: Turbine Technical Conference and Exposition. Volume 1A: Aircraft Engine; Fans and Blowers. *Düsseldorf, Germany*. June 16f, Germanydes. Proceedi
- Gun, G. (2016). Turbulence Model and Validation of Air Flow in Wind Tunnel. *International Journal of Technology* 7(8), 168-170.
- Heo, S., D. Kim and C. Cheong (2014). Analysis of Relative Contributions of Tonal Noise Sources in Volute Tongue Region of a Centrifugal Fan. *The Journal of the Acoustical Society of Korea* 33(1), 12-19.
- Jadhav, N. S. and S. R. Patil (2016). Effects of Volute Tongue Clearance and Rotational Speed on Performance of Centrifugal Blower. *International journal of scientific research in science, engineering and technology* 2(4), 261-266.
- Khelladi, S., S. Kouidri and Bakir, F. (2008). Predicting tonal noise from a high rotational speed 313(1-2), 113-133.
- Kind, R. J. and M. G. Tobin (1990). Flow in a Centrifugal Fan of the Squirrel-Cage Type. *Journal of Turbomachinery* 112(1), 84-90.
- Lee, Y. T. (2010). Impact of Fan Gap Flow on the Centrifugal Impeller Aerodynamics, *Journal of Fluids Engineering* 132(9), 91103-91103.
- Li, W., L. Xiao and Meng, W. (2020). *Effects of Bionic Volute Tongue on Aerodynamic Performance and Noise Characteristics of Centrifugal Fan Used in the Air-conditioner*, 17(4), 780-792.
- Lin, S. and C. Huang (2002). An integrated experimental and numerical study of forward-curved centrifugal fan. *Experimental Thermal and Fluid Science* 26(5), 421-434.
- Liu, X., M. Yuan and Y. Mao (2009). Numerical optimization of volute outlet structure for forward-curved centrifugal fan. HsiAnChiao Tung Ta Hsueh. *Journal of Xian Jiaotong University* 5(5), 012.
- Lun, Y. X., L. M. Lin and H. J. He (2019). Effects of vortex structure on performance characteristics of a multiblade fan with inclined tongue. *Proc IMechE A J Power Energy* 233(8), 1007 ower .
- Ning, K., X. Zhang, R. Guan, h. Guan, L. Qin, J. Huang, J. Guo and Y. Zhao (2010). CFD simulation and optimization of 9-26.5a high pressure centrifugal fan. *Mechanical design* 35 (S1), 155-158
- Patil, S. R., S. T. Chavan and N. S. Jadhav (2018). Effect of volute tongue clearance variation on performance of centrifugal blower by numerical and experimental analysis. *Materials Today: Proceedings* 5(2), 3883-3894.
- Sistek, V. (2015). Corotational and Compressibility Aspects Leading to a Modification of the Vortex-Identification Q-Criterion. *AIAA Journal* 53(8), 2406-2410.
- Suhrmann, J. F., D. Peitsch and Gugau, M. (2012). On the effect of volute tongue design on radial turbine performance[C]//Turbo Expo: Power for Land, Sea, and Air. *American Society of Mechanical Engineers*, 44748: 891-901.
- Sun, S. M., L. Q. Ren and T. Mei (2009). Practice and simulation analysis for reducing the centrifugal fan noise with bionics volute tongue. *Zhendong Yu Chongji. Journal of Vibration & Shock* 28(5), 32-34.
- Sun, Z., J. Zhou and H. Zhang (2007). On the Influencing Factors in a Pitot Tube Measurement I. Influence of Air Horn and Mounting Angle. *Chinese Journal of Sensors and Actuators* 20(3), 690-693.
- Ting, Z., Z. Cun and R. Gang (2012). Experimental Study on the Effect of Inclined Volute Tongue on the Noise *Reduction of Centrifugal Fan*. *Fluid Machinery* 10, 45-55
- Velarde-Suárez, S., R. Ballesteros-Tajadura, C. Santolaria-Morros (2008). Reduction of the aerodynamic tonal noise of a forward-curved centrifugal fan by modification of the volute tongue geometry. *Applied Acoustics* 69(3), 225-232.
- Wang, K., Y. Ju and C. Zhang (2018). A Quantitative Evaluation Method for Impeller-Volute Tongue Interaction and Application to Squirrel Cage Fan with Bionic Volute Tongue. *Journal of Fluids Engineering* 22,123-134.
- Wang, K., Y. P. YapingJu and C. H. Zhang (2021). Aerodynamic optimization of forward-curved blade centrifugal fan characterized by inclining bionic volute tongue. *Structural and Multidisciplinary Optimization* 130(9), 235-237.
- Wei, Y., L. Zhu and W. Zhang (2020). Numerical and experimental investigations on the flow and noise characteristics in a centrifugal fan with step tongue volutes. *Proceedings of the Institution of Mechanical Engineers, Part C: Journal of Mechanical Engineering Science* 234(15), 2979-2993.
- Wolfe, T., Y. T. Lee and M. E. Slipper (2015). A Performance Prediction Model for Low-Speed Centrifugal Fans. *Journal of Fluids Engineering* 137(5), 051106-051112.

- Wu, S. and Y. C. Fu (2013). Estimation of turbulent natural convection in horizontal parallel plates by the Q criterion. *International Communications in Heat and Mass Transfer* 45, 41-46.
- Xiong, Z., J. Deng, M. Wang, L. Yang and L. sun (2018). Influence of modified volute tongue design on aerodynamic performance of multi blade centrifugal fan. *Fan technology* 60 (06), 31-37
- Xu, C., M. Muller and W. J. Chen (2005). *Numerical Investigations of Volute Performance Due to Tongue Geometry*. 43rd AIAA Aerospace Sciences Meeting and Exhibit. Chichester, UK.
- Yang, H., P. Yu and J. Xu (2019). Experimental investigations on the performance and noise characteristics of a forward-curved fan with the stepped tongue. *Measurement & Control* 22, 1480-1488.
- Yang, J. (2018). *CFD numerical simulation and blade profile analysis of pressure characteristics of 9-26 centrifugal fan*. Wuhan University of technology, Wuhan, China.
- Zhang, B., S. Huang and Z. Sun (2006). Performance Improvement of Centrifugal Fan by Means of Numerical Simulation. *Chinese Journal of Mechanical Engineering* 019(001), 55-58.
- Zhang, J. H., W. L. Chu, H. G. Zhang, Y. H. Wu, and X. J. Dong (2016). Numerical and experimental investigations of the unsteady aerodynamics and aero-acoustics characteristics of a backward curved blade centrifugal fan. *Applied Acoustics* 110, 256-267.
- Zhang, N., J. X. Jiang, B. Gao and D. Ni (2020). Numerical analysis of the vortical structure and its unsteady evolution of a centrifugal pump. *Renewable Energy* 155, 748-760.
- Zhou H. and G. B. Ca (2017). *Research of wall roughness effects based on Q criterion*. *Microfluidics and Nanofluidics* 21(7), 114-121.
- Zhou, S. Q., H. X. Zhou and K. Yang (2021). Research on blade design method of multi-blade centrifugal fan for building efficient ventilation based on Hicks-Henne function. *Sustainable Energy Technologies and Assessments* 217(3), 100971 -100983.